Oxygen Reservoirs in the Early Solar Nebula Inferred from an Allende CAI

Edward D. Young* and Sara S. Russell

Ultraviolet laser microprobe analyses of a calcium-aluminum–rich inclusion (CAI) from the Allende meteorite suggest that a line with a slope of exactly 1.00 on a plot of $\delta^{17}O$ against $\delta^{18}O$ represents the primitive oxygen isotope reservoir of the early solar nebula. Most meteorites are enriched in ^{17}O and ^{18}O relative to this line, and their oxygen isotope ratios can be explained by mass fractionation or isotope exchange initiating from the primitive reservoir. These data establish a link between the oxygen isotopic composition of the abundant ordinary chondrites and the primitive ^{16}O-rich component of CAIs.

Nearly one-third of condensed matter in the inner solar system is composed of oxygen (*1*). Variability in $^{17}O/^{16}O$ and $^{18}O/^{16}O$ in samples of primordial oxygen from the early solar nebula therefore provides information about the precursors to the terrestrial planets. Grains of condensed mineral material within the accretion disk that surrounded the protosun tended to move inward radially toward the growing star. Protostellar accretion rates on the order of 1×10^{-5} to 1×10^{-8} solar masses ($M_\odot$) year^{-1} (*2–4*) suggest that the residence time of minerals inside 2 astronomical units (AU) (the region of terrestrial planet formation) may have been short in comparison with the life of the disk (*5*).

CAIs occur within chondrite meteorites and are the most primitive remains of the primordial solar nebula available for direct study. They formed from gas and dust progenitors of the solar system about 4.566 billion years before present (*6*), probably before terminal accumulation of the sun (*4*). Discovery of anomalously large concentrations of ^{16}O relative to ^{17}O and ^{18}O in CAIs (*7*) established that some of the oxygen from which these silicate and oxide materials are composed is distinct from oxygen typical of rocks in the solar system.

The linear array defined by the oxygen isotope ratios of CAI minerals on a three-isotope plot (*8*) is referred to as the CCAM line (carbonaceous chondrite anhydrous mineral line) (Fig. 1). It has a slope of 0.94 ± 0.02 as defined by CAI inclusions from the Allende CV carbonaceous chondrite meteorite (*9*), in contrast to mass fractionation curves with slopes slightly greater than 0.5. Mass fractionation curves result from mass-dependent isotope partitioning associated with physical and chemical processes. The slope of the CCAM line has been attributed to either mixing between end members with different amounts of ^{16}O through nucleosynthesis or mass-independent, symmetry-induced kinetic isotope partitioning among oxygen-bearing molecules in a gas phase (*10*). The oxygen isotopic compositions of solid materials from Earth and the moon define a single average mass fractionation curve on the three-isotope plot, termed the terrestrial mass fractionation curve (TF) (Fig. 1). The TF curve is representative of the terrestrial planets and related differentiated (melted) bodies of the inner solar system for which data exist; differentiated meteorites thought to be related to the terrestrial planets have oxygen isotope ratios within 0.5 $\delta^{17}O$ units of the TF curve (*11*).

Lack of colinearity among ordinary chondrites (OCs), representing primitive (unmelted) rock that was common in the nebula (*12*), and CAI minerals on the ^{16}O-rich and ^{16}O-poor ends of the CCAM line (Fig. 1), together with the relative positions of other solar system bodies on the three-isotope plot, implies the existence of at least three, and possibly more, primordial oxygen reservoirs during planetesimal formation in the early solar nebula. Existence of these reservoirs would have important implications for the origin of protoplanetary minerals and the state of the nebula before and during planet formation.

Twenty-two measurements of $^{17}O/^{16}O$ and $^{18}O/^{16}O$ from a coarse-grained type B1 CAI from Allende sample USNM 3576 (the inclusion is referred to hereafter as USNM 3576-1) were made with a spatial resolution of 100 μm and an analytical precision of ±0.1 to ±0.3 per mil with a method that combines in situ ultraviolet (UV) laser ablation and fluorination with gas-chromatography isotope ratio monitoring mass spectrometry (GCirms) (*13*).

USNM 3576-1 is a rounded, fully rimmed CAI that measured 2 cm by 0.5 cm before sampling and consists mainly of fassaite ($Al_2O_3 \simeq 18$ weight %, $TiO_2 \simeq 11$ weight %) and melilite ($Ak_{34\text{-}52}$). Magnesian spinel occurs as ubiquitous inclusions and is most abundant within and adjacent to fassaite. Anorthite ($An_{99\text{-}100}$) is also present. Fassaite crystals are generally enveloped by a mantle of anorthite and melilite about 100 μm wide. The outer 100-μm margin of the inclusion is composed of melilite with few other primary minerals in comparison with the interior. The mantles surrounding fassaite and the outer 100-μm margin of the inclusion have been altered (Fig. 2). Alteration consists of fine-grained nepheline, Na-bearing feldspar (An_{88}), and trace amounts of clinopyroxene. Iron enrichment of spinel (FeO up to 10 weight %) is also associated with the alteration at the inclusion margin. A Pb-Pb age of 4.5651 ± 0.0009 billion years was obtained for this inclusion (*5*).

Data from ablation pits in primary fassaite and melilite (Fig. 3) lie along a linear array with a best fit slope of 1.00 ± 0.03 and an intercept of −1.04 (correlation coefficient = 0.9998, Table 1). Because of the small grain size of the spinels relative to the diameter of the laser pits, all of the analyses include some spinel. The data are therefore affected by mixing with spinel as a result of laser sampling. The amount of spinel associated with the analyses is variable (Fig. 2 and Table 1). Spinel inclusions cause data for the host minerals to spread up and down the slope-1 line, indicating the absence of mass fractionation. The slope-1 line defined by primary fassaite, spinel, and melilite in USNM 3576-1 is coincident with a line connecting OCs and oxygen enriched in ^{16}O relative to OCs (Fig. 3).

Analyses from the altered zone at the melilite-rich, spinel-poor margin of the inclusion define a trend toward heavy O isotope enrichment (closed symbols in Fig. 3 and Table 1). The data are consistent with a slope-1/2 line, indicating that mass fractionation, rather than mixing of oxygen reservoirs, may have caused the heavy isotope enrichment (we will refer to this shallow-sloping trend as a mass fractionation line for simplicity). A single analysis of melilite from an altered zone almost completely enclosed by fassaite and containing almost no spinel (4-49 in Table 1 and a closed symbol in Fig. 3) is similar to the analyses from the spinel-poor altered margin of the inclusion. Analyses of the altered mantles that contain abundant spinel surrounding fassaite define a chord between the spinel-poor altered melilites and spinel + fassaite (crosses in Fig. 3 and Table 1). The chord is coincident with the CCAM line (Fig. 3).

Examination of the in situ laser ablation pits shows that the slope-1 and CCAM lines result from imperfect separation of high-^{16}O

E. D. Young, Department of Earth Sciences, University of Oxford, Parks Road, Oxford, OX1 3PR, UK. E-mail: ed.young@earth.ox.ac.uk S. S. Russell, Department of Mineralogy, Natural History Museum, Cromwell Road, London SW7 5BD, UK. E-mail: sarr@nhm.ac.uk

*To whom correspondence should be addressed.

and low-^{16}O components in the analyses and that it is the low-^{16}O phases that control the distinct slopes of the lines (*14*). Without the benefit of high spatial resolution afforded by the laser, the bulk oxygen isotope characteristics of USNM 3576-1 would appear similar to other CAIs; all of the data for the inclusion taken together define a line with a slope of 0.96 ± 0.02 and an intercept of −2.60 (*15*). The fluorination data for mineral separates that were originally used to define the CCAM line also represent mixtures of minerals (*9*), suggesting that the CCAM line may be an artifact, as it is in USNM 3576-1, of analyzing a mixture of different minerals. Distinction between the slope-1 line defined by unaltered minerals (Fig. 3) and the CCAM line may have gone undetected until now because such spatially specific variations in $^{17}O/^{16}O$ and $^{18}O/^{16}O$ as reported here would be difficult to detect in mineral separates (*16*). Secondary ion mass spectrometry methods, despite affording superior spatial resolution that allows analysis of separate minerals, generally lack the analytical precision required to distinguish between the two lines.

Laser ablation analyses of USNM 3576-1 show that oxygen isotope ratios related by different concentrations of ^{16}O (changes in $\delta^{17}O$ = changes in $\delta^{18}O$) and physicochemical alterations to those ratios ($\delta^{17}O$ and $\delta^{18}O$ varying in proportion to mass difference) are preserved in distinct parts of a single CAI. However, not all low-^{16}O phases lacking visible alteration in Allende CAIs lie on the slope-1 line rather than the CCAM line, implying that exchange or fractionation does occur in some unaltered primitive components. Laser ablation–fluorination–GCirms analyses of unaltered melilites from another, smaller type B1 CAI from the Allende 3576 stone, together with fassaite and spinel analyses, are on the CCAM line (*17*). Three conventional fluorination analyses of pyroxene separates relatively poor in ^{16}O are on the CCAM line (*9*, *18*).

We suggest that a single line with a slope of exactly 1, delimited by primary CAI phases in USNM 3576-1 and OCs, represents the primitive oxygen isotope reservoir of the early solar nebula. Almost all other analyzed planetary and meteoritic bodies are enriched in ^{17}O and ^{18}O relative to this line (Fig. 4), and their oxygen isotope ratios can be explained by mass fractionation or isotopic exchange initiating from the primitive reservoir. The proposed primordial array is consistent with either of two hypotheses for the origin of the ^{16}O anomalies in CAIs. The two hypotheses, mixing of older ^{16}O-enriched dust with younger ^{16}O-poorer dust and gas in the nebula (a two-component primordial reservoir) (*19*) and unmixing of oxygen by mass-independent reaction kinetics in the gas phase (a one-component primordial reservoir) (*20*), both predict a slope of 1.00.

The association between refractory CAIs and ^{16}O indicates that ^{16}O was abundant in a condensed form early in the history of the solar nebula. The first minerals of the nebula would have been resistant to mass fractionation because their small size would impede preservation of evaporative residues and there were no parent bodies to foster alteration by fluids. As these dust grains accreted, they experienced inward radial drift so long as they remained small (less than tens of centimeters in diameter) (*2*, *3*). During their protracted history, minerals with concentrated ^{16}O mixed with the more abundant ^{16}O-poorer oxygen represented by the OCs, giving rise to the slope-1 primordial array.

At some point in the evolution of the nebula, accreted rock bodies were of sufficient size to experience physicochemical processing of oxygen. Mass fractionation delimited by the laser ablation data for USNM

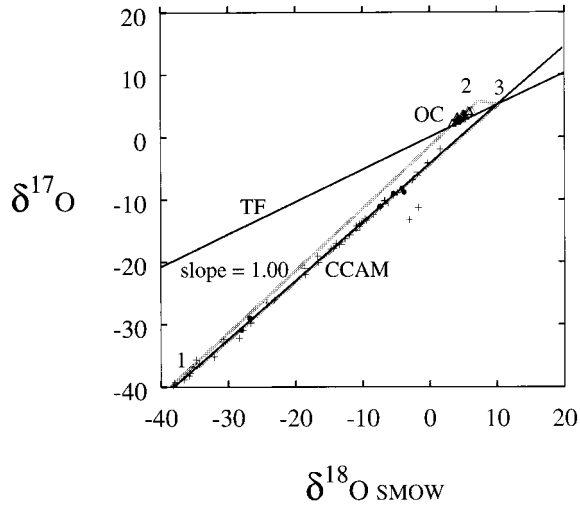

Fig. 1. Three-isotope plot for oxygen showing the positions of the TF line, the CCAM line, as represented by data in (*9*) (crosses) for the Allende CV carbonaceous chondrite, and the field for OCs, as represented by data in (*31*) (triangles). Closed circles are analyses of a type B1 CAI from Allende sample 3576 reported in (*17*). The corners of the grey triangle labeled 1, 2, and 3 represent the minimum number of distinct oxygen reservoirs in the early solar nebula if the CCAM line represents mixing between ^{16}O-rich material (but not pure ^{16}O, in the direction of 1) and ^{16}O-poor material (*4*) without modification by physicochemical mass-dependent fractionation. The isotopic compositions of protoplanetary minerals would fall within the region bounded by the gray triangle if the CCAM is attributable to mixing without fractionation. The two CAI data points to the right of the CCAM are from a FUN inclusion (FUN refers to fractionation and unidentified nuclear effects) (*9*).

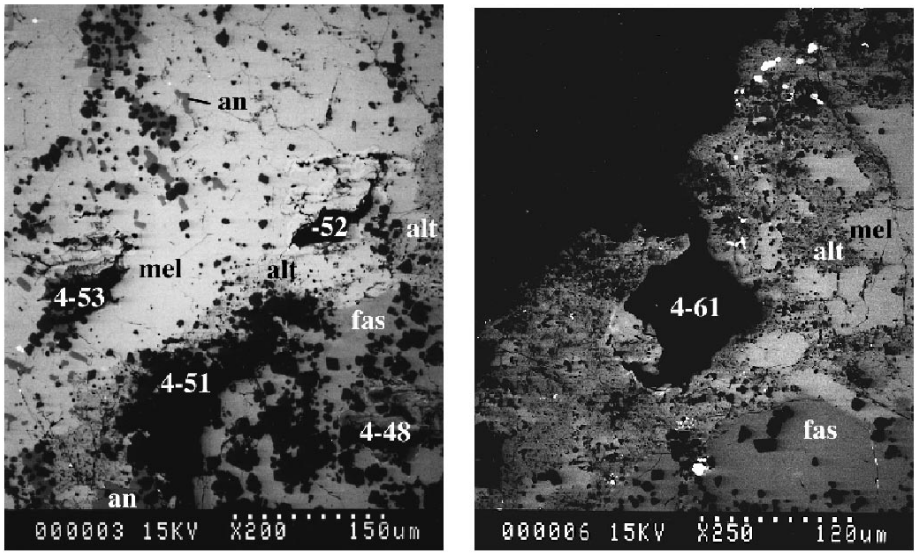

Fig. 2. Backscattered electron images of the regions surrounding laser ablation pits 4-48, 4-51, 4-52, and 4-53 (**left**) and 4-61 (**right**). The images are of a thin section of the sample cut after laser sampling. The thin section thickness of 30 μm is comparable to the depth of the uneven laser pit floors. The latter thus show up as wavy banded patterns marred by irregular black holes in the section. The size of pit 4-51 is exaggerated by plucking out of material during sectioning. Melilite (mel) appears bright in these images. Fassaite (fas) shows up as the intermediate gray tone, whereas ubiquitous spinel (concentrated in pyroxene) is manifest as black euhedral grains. Alteration of melilite by Na-bearing minerals (alt) appears as mottling on melilite. Anorthite (an) appears as a gray tone darker than fassaite in the left image. Note anorthite in the altered zone surrounding fassaite at the bottom of the left image.

3576-1 and isotopic measurements of other chondrite components (*21*, *18*) may mark this crucial time. Enrichment in ^{17}O and ^{18}O along mass fractionation lines (for example, Fig. 3) could be the result of oxygen exchange between condensed minerals and volatiles at low temperatures (<300°C) or evaporation of condensed phases at high temperatures (>700°C) (*22*, *23*).

There is a positive correlation between mass fractionation of oxygen isotopes (^{17}O and ^{18}O enrichment along a shallow slope) and Na metasomatism in USNM 3576-1. It is conceivable that Na, ^{17}O, and ^{18}O were introduced into the CAI while in the parent body by an aqueous fluid flowing through fractures and grain boundaries (*24*), but aqueous alteration cannot be a general explanation for the different slopes of the slope-1 and CCAM lines because not all unaltered phases lie on the slope-1 line. Partial evaporation of melilite at the rim of the inclusion and evaporation of melilite and feldspar (or their precursors) adjacent to pyroxene grains could have caused the ^{17}O and ^{18}O enrichment along a slope-1/2 line and hence displacement from the slope-1 line to the position of the CCAM line, without necessarily involving alkali enrichment. Evaporative oxygen isotope effects in solid or molten melilite are plausible with even the most transient exposures to high temperatures in the solar nebula (*25*). Coexisting pyroxene and spinel would remain unaffected because at these temperatures their oxygen diffusivities are four orders of magnitude smaller than that for melilite (*26*).

Melilite-fassaite interfaces should melt at lower temperatures than melilite (*27*). Partial melting near pyroxene would enhance the opportunity for evaporative isotope effects and could explain the localized occurrence of oxygen isotope fractionation. The presence of anorthite preferentially near pyroxene may be the result of crystallization of an interstitial melt (*27*). While molten, reductions in temperature or enrichments in dust relative to gas would have driven gaseous Na into the liquid phase (*28*), thus accounting for the correlation between Na and oxygen isotope fractionation in USNM 3576-1. If Na metasomatism is the result of heating, then Na and oxygen

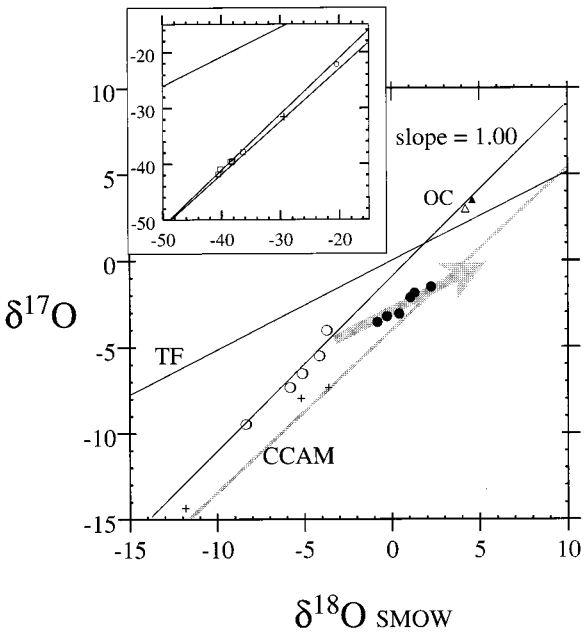

Fig. 3. Three-isotope plot showing the UV laser ablation in situ analyses of inclusion USNM 3576-1. Data with $\delta^{18}O < -15$ per mil are shown in the inset at top left. Open circles represent unaltered melilite > spinel, solid circles represent altered melilite with negligible amounts of spinel that occur along the edge of the inclusion and in one instance adjacent to fassaite, crosses are altered melilite + anorthite analyses that include substantial amounts of spinel (and in one case fassaite), and boxes are fassaite > spinel (fas + sp). The gray arrow draws attention to the mass fractionation trajectory of the spinel-poor altered melilite data. The altered melilite with abundant spinel (± fassaite, crosses) forms a chord coincident with the CCAM line (gray line). The average compositions of L and H ordinary chondrites from the literature (open and closed triangles, respectively) are also shown. The line labeled slope = 1.00 is the best fit to unaltered minerals from USNM 3576-1 and is coincident with a mixing line between ordinary chondrites and a reservoir enriched in ^{16}O. The TF, slope-1, and CCAM lines are all shown in the inset at top left, from top to bottom.

Table 1. Results of in situ laser ablation oxygen isotope ratio analysis of CAI inclusion USNM 3576-1. All values for $\delta^{18}O$ and $\delta^{17}O$ are relative to SMOW.

Run	Minerals*	$\delta^{18}O$†	$\delta^{17}O$‡	$F^{17}O$§
4-47	mel + alt ≫ sp, edge	1.05	−2.14	−2.15
4-48	fas > sp	−38.52	−39.59	−0.03
4-49	mel + alt ≫ sp	−0.28	−3.24	−1.92
4-50	fas > sp	−38.20	−39.54	−0.30
4-51	mel + an + alt + sp	−11.83	−14.35	−1.48
4-52	mel + alt > sp	−5.19	−7.98	−1.75
4-53	mel + sp ≫ an	−8.34	−9.47	−0.09
4-54	mel ≫ sp	−3.70	−4.04	0.70
4-55	mel + sp	−20.46	−22.2	−0.70
4-56	mel ≫ sp	−5.11	−6.53	−0.38
4-57	fas > sp	−40.60	−41.86	−0.22
4-58	fas > sp	−40.22	−40.97	−0.30
4-59	fas > sp	−38.24	−39.68	−0.40
4-60	mel + alt ≫ sp, edge	−0.83	−3.56	−1.69
4-61	mel + alt ≫ sp, edge	2.24	−1.53	−2.73
4-63	mel + alt ≫ sp, edge	0.42	−3.09	−2.47
4-64	mel + alt > sp, edge	−3.63	−7.35	−2.68
4-65	mel + alt ≫ sp, edge	1.30	−1.89	−2.15
4-66	mel ≫ sp	−4.12	−5.51	−0.35
4-67	fas + mel + alt > sp	−29.41	−31.57	−1.12
4-68	fas > sp	−36.37	−37.87	−0.46
4-69	mel ≫ sp	−5.81	−7.34	−0.49

*Mineral abbreviations are as follows: mel, melilite; fas, fassaite; sp, spinel; alt, ± Na-plagioclase ± nepheline ± clinopyroxene; and an, anorthite. Qualitative relative abundances are indicated by inequalities. Edge refers to analyses of the margin within 100 μm of the inclusion edge. †Estimated precision is ±0.2 per mil (1σ). ‡Estimated precision is ±0.2 per mil (1σ). §$F^{17}O = \delta^{17}O - [1.00(\delta^{18}O) - 1.044]$ and is the deviation from the best fit line through data for unaltered zones.

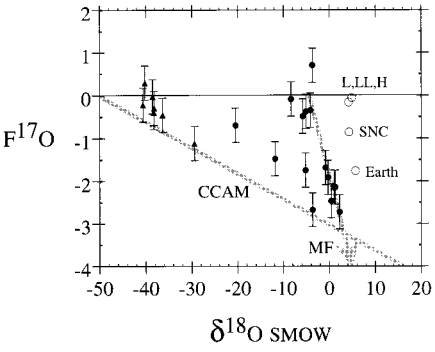

Fig. 4. Plot of deviations in $\delta^{17}O$ from the best fit line through the data $\{F^{17}O = \delta^{17}O - [1.00(\delta^{18}O) - 1.044]\}$ for unaltered minerals in USNM 3576-1 against $\delta^{18}O$. Solid circles represent melilite ± anorthite ± spinel, whereas triangles represent fassaite + spinel (4-67 includes melilite). The extent of mass fractionation, represented by the arrow labeled MF, is substantially larger than the uncertainties in the measurements (error bars depict 2σ) and is comparable to the differences in $^{17}O/^{16}O$ and $^{18}O/^{16}O$ among H, L, and LL ordinary chondrites, Mars (SNC achondrite meteorites, named after the Shergotty, Nakhla, and Chassigny type examples), and Earth (shown as labeled open circles). Laser sampling of mixtures of ^{16}O-rich and ^{16}O-poor minerals (points near the middle of diagram, see Table 1) results in the shallow negative sloping CCAM line.

isotope fractionation at the melilite-rich inclusion margin requires that such a heating event was short-lived. Otherwise, the entire CAI (excluding refractory spinel) would have melted and been altered (*29*).

The picture that emerges from the laser ablation analyses of $^{17}O/^{16}O$ and $^{18}O/^{16}O$ in USNM 3576-1 is that the solar system precursor oxygen was variable in ^{16}O but otherwise well mixed. The slope-1 array on the oxygen three-isotope plot is common to primitive chondrite meteorites in general and is a vestige of the original heterogeneity in ^{16}O concentration in the primordial solar nebula. Discrete parts of CAIs were subjected to evaporation or other agents of chemical and isotopic change (or to both) that altered the primordial $^{17}O/^{16}O$ and $^{18}O/^{16}O$.

References and Notes

1. Roughly 70 to 80% by mass of each of the terrestrial planets is composed of a silicate mantle. These mantles are composed of 48% by mass oxygen [H. Wänke and G. Dreibus, *Philos. Trans. R. Soc. London A* **325**, 545 (1988); K. Lodders and B. Fegley Jr., *Icarus* **126**, 373 (1997)]. The abundant OC meteorites are composed mainly of silicates and oxides, suggesting that the same is true for much of the asteroid belt (*30*).
2. A. P. Boss, *Astrophys. J.* **417**, 351 (1993).
3. _____, *ibid.* **469**, 906 (1996); J. N. Cuzzi, A. R. Dobrovolskis, J. M. Champney, *Icarus* **106**, 102 (1993).
4. A. G. Cameron, *Meteoritics* **30**, 133 (1995).
5. Astronomical observations of young stellar objects together with mathematical simulations suggest that early in its evolution the protosun accreted at a rate of $1 \times 10^{-5}\ M_\odot\ \text{year}^{-1}$ (*4*). If the circumstellar disk was a steady-state source for the growing nebular core (*2*), then material within 2 AU of the growing star would have been consumed every 80 years on the basis of a canonical disk mass of 0.02 $M_\odot$ and the assumption that the source of the accreting matter was the disk. Once the protosun entered a T Tauri phase, accretion is thought to have slowed to $\sim 1 \times 10^{-8}\ M_\odot\ \text{year}^{-1}$ and persisted for several million years (*4*). For a canonical disk mass and assuming that the sole source of accretion was the disk, material within 2 AU would have been consumed every 80,000 years during this interval.
6. C. J. Allègre, G. Manhès, C. Göpel, *Geochim. Cosmochim. Acta* **59**, 1445 (1995). The Pb-Pb date for inclusion USNM 3576-1 was reported as sample A1/7 in their study.
7. R. N. Clayton, L. Grossman, T. K. Mayeda, *Science* **182**, 485 (1973).
8. On a three-isotope plot, $\delta^{17}O$ (ordinate) is plotted against $\delta^{18}O$ (abscissa). $\delta^{17}O$ refers to the per mil deviation in a sample $^{17}O/^{16}O$ from a standard, in this case standard mean ocean water (SMOW), expressed as $\delta^{17}O = [(^{17}O/^{16}O)_{\text{sample}}/(^{17}O/^{16}O)_{\text{SMOW}} - 1] \times 1000$. Values of $\delta^{18}O$ are defined in an analogous fashion.
9. R. N. Clayton, N. Onuma, L. Grossman, T. K. Mayeda, *Earth Planet. Sci. Lett.* **34**, 209 (1977).
10. R. N. Clayton, *Annu. Rev. Earth Planet. Sci.* **21**, 115 (1993).
11. A derivation of the relation between $\delta^{17}O$ and $\delta^{18}O$ that defines the TF curve is given by Y. Matsuhisa, J. R. Goldsmith, and R. N. Clayton [*Geochim. Cosmochim. Acta* **42**, 173 (1978)] in their appendix 1. It is the result of a 2:1 mass difference ratio between ^{18}O and ^{17}O relative to ^{16}O. Homogeneity in Earth's initial oxygen reservoir is supported by lack of deviations from the average TF curve [F. Robert, A. Rejou-Michel, M. Javoy, *Earth Planet. Sci. Lett.* **108**, 1 (1992)]. The relation between the average TF curve and other rocky bodies of the solar system is summarized in (*31*).
12. Recent studies of "space weathering" of asteroids (*30*) suggest that the dominance of OCs among the stony meteorites reflects the profusion of this material in the asteroid inner main belt and, by inference, in the protoplanetary inner solar system.
13. The UV laser ablation and fluorination method for measuring $^{18}O/^{16}O$ and $^{17}O/^{16}O$ in situ is described in detail elsewhere (*17*). Combining UV laser ablation with GCirms offers the capability to analyze exceptionally small portions of O_2 (10 to 20 nmol) with accuracy and precision similar to other fluorination methods that normally require several micromoles of analyte. Accuracy and precision of the laser-based oxygen isotope analytical method were determined by analyzing terrestrial standards and a smaller Allende CAI (*17*). In the present study, seven analyses of a specimen of augite pyroxene (USNM 133866) yielded a mean $\delta^{18}O$ of 5.8 ± 0.3 (1σ) per mil and a mean $\delta^{17}O$ of 2.9 ± 0.1 (1σ) per mil relative to SMOW. Two conventional fluorination analyses of this same pyroxene performed by A. G. Hunter at the Natural Environment Research Council Isotope Geosciences Laboratory, United Kingdom, gave $\delta^{18}O$ values of 6.0 and 5.9 per mil relative to SMOW. Conventional analyses of the NBS-28 quartz standard run with the pyroxene sample gave a $\delta^{18}O$ value of 9.7 per mil relative to SMOW. Mass fractionation suggests that $\delta^{17}O$ for augite USNM 133866 should be 3.0 per mil relative to the measured $\delta^{18}O$ of 5.8 per mil. These data suggest an accuracy of ± 0.2 per mil or better and a precision of between ± 0.1 and ± 0.3 per mil at the time inclusion USNM 3576-1 was analyzed.
14. The CCAM and slope-1 lines converge at $\delta^{18}O$ values less than about -30 per mil, values typical of spinel and most (but not all) fassaites, and differences among individual inclusions (presumably in part due to sampling) cause up to 0.5 per mil ambiguity in the $\delta^{17}O$ of lines defined by the inclusions at $\delta^{18}O$ of -30 per mil (*9*).
15. Best fit lines for anhydrous minerals in carbonaceous chondrites vary. The equation for the CCAM line as commonly defined is based on data for Allende (*9*) and is $\delta^{17}O = 0.94 \pm 0.02(\delta^{18}O) - 4.2$. The line defined by fluorination analyses of anhydrous mineral separates for the Murchison carbonaceous chondrite yields a best fit equation of $\delta^{17}O = 0.95 \pm 0.04(\delta^{18}O) - 3.4$ [R. N. Clayton and T. K. Mayeda, *Earth Planet. Sci. Lett.* **67**, 151 (1984)].
16. Characteristic x-ray maps and backscattered electron images reveal the presence of localized patches of submicron alteration in otherwise pristine melilite throughout inclusion USNM 3576-1.
17. E. D. Young, D. W. Coutts, D. Kapitan, *Geochim. Cosmochim. Acta*, in press.
18. T. K. Mayeda, R. N. Clayton, H. Nagasawa, *Lunar Planet. Sci. Conf.* **XVII**, 526 (1986).
19. R. N. Clayton *et al.* proposed (*7*) that the CCAM line is the result of incorporation of pure ^{16}O of interstellar origin. The definition of δ requires that mixtures of pure ^{16}O with oxygen having any $^{17}O/^{16}O$ and $^{18}O/^{16}O$ will result in a mixing line with a slope of exactly 1.00. More recently, absence of pure ^{16}O carrier grains in meteorites [L. R. Nittler, C. M. O. Alexander, X. Gao, R. M. Walker, E. Zinner, *Astrophys. J.* **483**, 475 (1997)] has engendered the notion that the ^{16}O component was interstellar dust derived from older stellar sources of less overall metal (heavy element) content relative to the remainder of the nebula (*32*). Because the nucleosynthesis of ^{16}O does not rely on the heavy elements (such as C and O), whereas the production of ^{17}O and ^{18}O does, average galactic oxygen will have progressively less ^{16}O relative to ^{17}O and ^{18}O over time. Refractory solids rich in Al can persist in the interstellar medium for 10^8 to 10^9 years (*33*). As a result of their low volatility, the average age of interstellar Al_2O_3 grains is expected to be greater than the mean bulk material age at any given time. Because they grew from atoms synthesized earlier in the history of the galaxy, refractory solids rich in Al may be enriched in ^{16}O (*32, 33*). Ancient, Al-rich dust could have been the progenitor of the ^{16}O-rich signal in CAIs. In this scenario, the ^{16}O progenitor is not pure but nevertheless differs from the ^{16}O-poorer oxygen by the abundance of ^{16}O alone, yielding a slope of 1.00 on a three-isotope plot.
20. Experiments [J. Wen and M. H. Thiemens, *J. Geophys. Res.* **98**, 12801 (1993)] show that the magnitude of $^{17}O/^{16}O$ and $^{18}O/^{16}O$ differences between the most ^{16}O-rich components of CAIs and OCs is similar to the symmetry-induced kinetic isotope effects (so-called mass-independent fractionation) that occur among oxygen-bearing species in some gas-phase reactions. Upon achieving steady state, such reactions can generate products that are enriched in ^{16}O relative to the initial uniform isotopic composition of the reservoir gas. The result is an unmixing line with a slope of precisely 1 on a plot of $\delta^{17}O$ (ordinate) versus $\delta^{18}O$ (abscissa) spanning several tens of per mil in δ values. M. H. Thiemens has argued in numerous publications [see M. H. Thiemens, in *Isotope Effects in Gas-Phase Chemistry*, J. A. Kaye, Ed. (American Chemical Society, Washington, DC, 1992), vol. 502, chap. 9, pp. 138–154] that mass-independent gas-phase reactions involving rock-forming species such as SiO could explain ^{16}O enrichment of CAIs relative to other rocky components of the solar system.
21. I. Jabeen, M. Kusakabe, T. Nakamura, K. Nagao, *Meteorit. Planet. Sci.* **33**, A76 (1998); K. D. McKeegan, L. A. Leshin, G. J. MacPherson, *ibid.*, p. A102.
22. N. Onuma, R. N. Clayton, T. K. Mayeda, *Geochim. Cosmochim. Acta* **36**, 169 (1972).
23. E. D. Young, H. Nagahara, B. O. Mysen, D. M. Audet, *ibid.*, in press.
24. S. S. Russell *et al.*, *ibid.* **62**, 689 (1998).
25. Fully implicit finite difference solutions to the diffusion equation with the boundary conditions imposed by volatilization were obtained to simulate the kinetic isotope effects of free evaporation of melilite. The equations and method of solution are described in (*23*). Calculations were performed for a spherical grain of solid melilite and a droplet of liquid, each with an initial radius of 0.25 cm evaporating at 1400° or 1500°C, respectively. Oxygen diffusivity for the solid melilite was taken to be $1 \times 10^{-10}\ \text{cm}^2\ \text{s}^{-1}$. Oxygen diffusivity for the melt was taken to be $2 \times 10^{-6}\ \text{cm}^2\ \text{s}^{-1}$. Both diffusivities are from (*26*). The liquid rate of evaporation of $-1 \times 10^{-4}\ \text{cm s}^{-1}$ was suggested by the forsterite experimental data of A. M. Davis, A. Hashimoto, R. N. Clayton, and T. K. Mayeda [*Nature* **347**, 655 (1990)]. The solid rate of evaporation of $-3 \times 10^{-8}\ \text{cm s}^{-1}$ corresponds to that of solid SiO_2 and is an order of magnitude slower than the rate for solid forsterite (*23*). The oxygen isotope fractionation factor for $^{18}O/^{16}O$ was taken to be 0.983, as prescribed by the weighted average of the square root of inverse mass ratios for the isotopomers of SiO_2, 2(CaO), and Al_2O_3 (that is, the model melilite was gehlenite). Results were integrated over the outer 50 μm of the residual spherical material for comparison with laser ablation sampling. Results show that the outer 50 μm of solid melilite exhibits a shift in $\delta^{18}O$ of $+5.7$ per mil in 36 hours, whereas the outer edge of the molten sphere is shifted by $+17.2$ per mil in 15 min. The smaller oxygen diffusivities of O in solid pyroxene and spinel make preservation of heavy isotope enrichment in their evaporative residues unlikely.
26. F. J. Ryerson and K. D. McKeegan, *Geochim. Cosmochim. Acta* **58**, 3713 (1994).
27. S. Yoneda and L. Grossman, *ibid.* **59**, 3413 (1995).
28. D. S. Ebel and L. Grossman, *Lunar Planet. Sci. Conf.* **XXIX** (1998) [CD-ROM]; J. M. Allen, L. Grossman, A. M. Davis, I. D. Hutcheon, *ibid.* **IX**, 1209 (1978).
29. Large differences in temperature could be sustained for no more than a few tens of seconds because length scales for thermal diffusion in mineral materials are comparable to the size of the CAI over this time scale; either heating was on the order of a second, or kinetic barriers must have existed if partial melting was confined to the rim of the inclusion and mantles surrounding fassaite.
30. C. R. Chapman, *Meteorit. Planet. Sci.* **31**, 699 (1996).
31. R. N. Clayton, N. Onuma, T. K. Mayeda, *Earth Planet. Sci. Lett.* **30**, 10 (1976).
32. D. D. Clayton, *Astrophys. J.* **334**, 191 (1988).
33. _____ and K. Liffman, *ibid.* **346**, 531 (1989).

34. Funding was provided by an award from the National Environment Research Council, UK. USNM 3576-1 was supplied by J. Arden.

1 July 1998; accepted 14 September 1998